Journal of Quantitative Spectroscopy & Radiative Transfer 284 (2022) 108166

Contents lists available at ScienceDirect

Journal of Quantitative Spectroscopy & Radiative Transfer

journal homepage: www.elsevier.com/locate/jqsrt

Enhanced optical chirality with directional emission of Surface Plasmon Polaritons for chiral sensing applications

Guillermo Serrera[a], Javier González-Colsa[a], Vincenzo Giannini[b,c,d], José M. Saiz[a], Pablo Albella[a,*]

[a] Group of Optics, Department of Applied Physics, University of Cantabria, 39005, Santander, Spain
[b] Instituto de Estructura de la Materia (IEM), Consejo Superior de Investigaciones Científicas (CSIC), Serrano 121, 28006 Madrid, Spain
[c] Technology Innovation Institute, Building B04C, Abu Dhabi P.O. Box 9639, United Arab Emirates
[d] Centre of Excellence ENSEMBLE3 sp. z o.o., Wolczynska 133, Warsaw, 01-919, Poland

ARTICLE INFO

Article history:
Received 15 January 2022
Accepted 11 March 2022
Available online 12 March 2022

Keywords:
Enhanced Chirality
All-Dielectric Metasurface
Sensing
Plasmon
Nanoantenna

ABSTRACT

Chirality is a crucial aspect in life sciences, where systems capable of enhancing the chiroptical properties of molecules are highly demanded. In this work, we present a numerical proof of concept of a novel approach towards chiral sensing, consisting in the measurement of chiroptical properties via the directional emission of Surface Plasmon Polaritons (SPPs) on a metasurface. Based on the enhanced differential absorption between right and left circularly polarized light upon interaction with a metasurface made of high refractive index dielectric unit cells, a polarization-dependent SPP differential emission is obtained. Furthermore, the plasmonic emission direction is entirely dependent on the polarization handedness. Using FDTD numerical methods we report Circular Dichroism signals of around − 6° for the unit cell, with threefold dissymmetry factor enhancements in places accessible to analytes. We believe that this work sets a brand-new branch in chiral sensing towards faster, real-time measurements.

1. Introduction

The concept of chirality refers to the difference between a given object and its mirror image, even under consideration of all possible translation and rotation combinations in that object. In other words, it is the lack of mirror symmetry inside that object for any arbitrary plane. This results in the presence of a certain kind of handedness in that object, where the two different mirror images stemming from this lack of symmetry, called enantiomers, cannot be superimposed [1,2]. Chirality is a property found in many objects in nature, particularly in microscopic components that are relevant in life sciences, such as sugars, amino acids, and enzymes [3]. The geometrical difference that appears with chiral elements does not affect the various physical and chemical properties of a compound, i. e., thermal and electrical conductivities, mass or density; provided that they are immersed in an achiral medium. However, when in contact with other chiral elements, as often occurs in biological systems [4,5], interactions may differ greatly. For instance, changes in chirality have been suggested as the underlying origin for Alzheimer and Parkinson's diseases [6]. Furthermore, pharmacological compounds, which are often chiral, may display different effects on the human body depending on the enantiomer that is present. One example of this was the use of thalidomide, where one of the enantiomers caused fetus damage in pregnancies [7–9]. Therefore, there is a growing interest in the pharmacological industry towards single-enantiomer drugs, where effectiveness, availability and metabolism can be improved, as well as the reduction of the potential unwanted side effects. In order to attain this, identification and separation of enantiomers is a key aspect.

The identification of the chirality of a molecule sample is typically performed via Circular Dichroism (CD) spectroscopy, where the absorption difference of the molecules between right and left-circularly polarized light (CP) beams is measured [10]. However, the CD effects in raw samples are inherently weak and therefore high concentrations and long measurement times are required. In order to bypass these issues, nanostructures can be engineered so that the chiroptical interaction with the molecule sample is enhanced [11]. One approach towards this is the use of plasmonic nanoparticles (NPs), which allows for large field enhancements

* Corresponding author.
E-mail address: pablo.albella@unican.es (P. Albella).

https://doi.org/10.1016/j.jqsrt.2022.108166

at the interphase with the medium [12–22]. Despite this large enhancement, ohmic losses in these materials are considerable, leading to a substantial heating of the sample which may affect the CD measurements and damage the molecules, thus hindering the potential practicality of these devices.

Another recent approach, constituting an alternative to these plasmonic materials, is the use of high refractive index (HRI) dielectric materials [23]. Their low losses and magnetic-electric multipolar responses [24–28] can be exploited for applications in spectroscopy, sensing or light guiding, among others [29–32]. Chiral studies have already been performed in all-dielectric metasurfaces, where the chiroptical response has been shown to be greatly enhanced [33–37]. Despite this, practical implementation of many of these metasurfaces seems unlikely due to fabrication limitations. Studies with achiral unit cells such as spherical NPs show that, despite their capability to provide high local chirality absorption differences (measured with the Kuhn dissymmetry factor g), the overall enhancement of the CD effect is small [38]. To further amplify the CD effect, the introduction of chiral unit cells has been proposed recently, achieving giant CD signals by using all-dielectric gammadion bilayers [15]. Nonetheless, most of the structures showing extreme enhancements of the CD effect are embedded in other materials, hampering their use with actual molecule samples. Another issue that stems from the use of chiral unit cells is the noise introduced by the chiral cell into the CD signal, which can be circumvented using racemic metasurfaces (with same proportion for both rotating modes), as shown by R. Quidant et al [22]. Furthermore, many HRI structures display hotspots located inside the material, again hindering actual sensing applications. Thus, nanostructures capable of offering an overall effective enhancement of the CD effect, with external hotspots accessible to molecules, are sought.

An important technology in all areas of biosensing is the use of Surface Plasmon Resonances (SPR) due to its real-time responses and non-intrusive nature [39,40]. The ability of Surface Plasmon Polaritons (SPP) to detect changes in the refractive index of neighboring media has been demonstrated, in both Attenuated Total Reflection (ATR) and diffraction grating coupling approaches [41,42]. Particularly, Kretschmann-Raether couplers have been demonstrated to be able to detect the chiral properties of samples via angle-resolving [43]. However, the absence of chiral elements in such a configuration limits its performance in chiral sensing. Grating SPP couplers, which allow for normal illumination, have not been considered for this purpose yet, to the best of our knowledge. However, their necessity of a metasurface above the metal layer allow for the introduction of chiral elements, which could be exploited to enhance the chiroptical effects of the structure. Recent works also show that the propagation of plasmons in a grating coupler can be controlled with the incident polarization of light [44]. Given the polarization dependency of the CD effect, the directional emission of plasmons from the grating could contain the chiral information of the sample, allowing for a real-time, enhanced chiroptical response from the device.

Here, we show the proof of concept of such a device, a metasurface that offers a high chiroptical response, as well as the ability to selectively launch Surface Plasmon Polaritons in a particular direction depending on the incident polarization. The scheme behind this device is illustrated in Fig. 1. A S-like shaped structure made of a HRI dielectric material is considered as unit cell for the structure. This system can offer both a high far-field unit cell CD signal and large local chirality over significant areas. The unit cells are organized in a double column grating pattern and placed above glass ($n_g = 1.5$) and gold layers in order to support SPP generation. The overall structure is surrounded by air. Results were obtained by numerically solving Maxwell's equations using a commercial 3D-FDTD method (Lumerical).

2. Theory

The absorption rate of light at frequency ω by a chiral molecule was described by Tang and Cohen [45,46]

$$A^{\pm} = \boldsymbol{E}\cdot\dot{\boldsymbol{p}} + \boldsymbol{B}\cdot\dot{\boldsymbol{m}} = \frac{\omega}{2}\left(\alpha''\left|\tilde{\boldsymbol{E}}\right|^2 + \chi''\left|\tilde{\boldsymbol{B}}\right|^2\right) \mp \frac{2}{\varepsilon_0}G''C \tag{1}$$

where the + and – signs refer to right and left CP light respectively. $\boldsymbol{p}$ and $\boldsymbol{m}$ are the electric and magnetic dipole moments, that depend not only on the electric and magnetic complex polarizabilities $\tilde{\alpha}$ and $\tilde{\chi}$, but also on a mixed electric-magnetic dipole polarizability $\tilde{G}$. Here, the $''$ superindex stands for the imaginary part of such polarizabilities. ε_0 is the usual vacuum permittivity and the remaining C term, dependent only on the electromagnetic field, is the chiral state density, defined as

$$C = \frac{\varepsilon_0}{2}E\cdot(\nabla\times\boldsymbol{E}) + \frac{1}{2\mu_0}B\cdot(\nabla\times\boldsymbol{B}) = -\frac{\omega\varepsilon_0}{2}\Im\mathfrak{m}\left(\tilde{\boldsymbol{E}}^*\cdot\tilde{\boldsymbol{B}}\right) \tag{2}$$

where μ_0 is the vacuum magnetic permeability. As the CD effect is the difference in absorption between right and left CP, it can be seen that the effect can be quantified from the difference in the second term in Eq. (1), as $A^+ - A^- = -\frac{4}{\varepsilon_0}G''C$, making the CD effect proportional to the chiral state density. It can also be seen that this quantity is dependent on polarization, reaching in vacuum a maximum value for circular polarization of

$$C_{CP} = \pm\frac{\omega\varepsilon_0}{2c}\left|\tilde{\boldsymbol{E}}\right|^2 \tag{3}$$

where c is the speed of light and the + and – signs refer again to the handedness. Manipulation of the electromagnetic field through engineering of nanoantennae is therefore capable of enhancing the averaged chiral density of states over the CP value allows for magnification of the CD effect.

The differential absorption between polarizations in chiral media can also be quantified using the dissymmetry factor, which takes the absorption difference in the Tang-Cohen formalism and normalizes it to the total absorption rate (taken as the average value $(A^+ + A^-)/2$):

$$g = 2\frac{A^+ - A^-}{A^+ + A^-} \approx -8\left(\frac{G''}{\alpha''}\right)\left(\frac{C}{\omega\varepsilon_0\left|\tilde{\boldsymbol{E}}\right|^2}\right) \tag{4}$$

where the magnetic term in Eq. (1) has been neglected with respect to the electric and mixed terms. Due to its dependence on C, this factor takes a maximum value $g_{CP} = -\frac{4}{c}\left(\frac{G''}{\alpha''}\right)$ for CP, but can be improved by means of nanostructure engineering. For this purpose, it is useful to define the CP-normalized dissymmetry factor $\hat{g}$, a normalized form with respect to the CP value that is sought to be surpassed:

$$\hat{g} = \frac{g}{g_{CP}} = \pm c\frac{\Im\mathfrak{m}\left(\tilde{\boldsymbol{E}}^*\cdot\tilde{\boldsymbol{B}}\right)}{\left|\tilde{\boldsymbol{E}}\right|^2} \tag{5}$$

As can be observed from this equation, the normalized absorption difference can be enhanced by means of an increment of the chiral density of states or a reduction of the total electric field.

Directional emission of SPPs can be achieved by considering unit cells with a privileged direction in a double column grating [44]. One column must be oriented at an angle θ_1 and the other at a perpendicular angle θ_2. An appropriate shaping for the unit cells allows coupling to the incident electric field component that is perpendicular to the privileged direction of the unit cell. A dipole emission pattern is then formed in each unit cell, and the constructive interaction between dipoles in a single column of the structure create the SPP. This propagates along the perpendicular direction of the column. For simplicity we will hereon consider y-oriented columns, making the plasmons propagate along the x-axis direction, right or left.

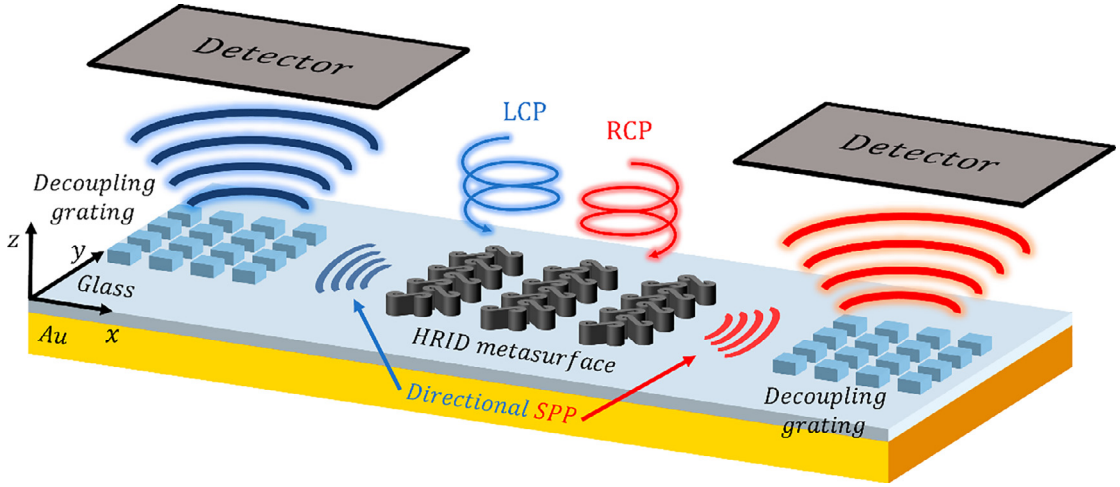

Fig. 1. Scheme of the proposed device. Circularly polarized beams impinge the HRI dielectric chiral metasurface, on which the sample is put. This generates SPPs directionally, with the plasmon intensity dependent on the absorption by the sample, enhanced by the metasurface, particularly at the high local chirality areas. The SPPs propagate across the substrate until they reach a decoupling grating system, which transforms the SPP back into a wave that can be detected.

Since there are two columns with different orientations in the grating, an arbitrary incident electromagnetic wave may have its electric field coupled to both columns. This means that the emerging plasmon will have contributions from both columns, as well as some cross terms arising from the interaction between them. The plasmonic intensity at either side of the grating is given by the following expression

$$I_L \propto \left(Q_1 E_1^2 + Q_2 E_2^2\right) + 2E_1 E_2 \cos\left(k_{SPP} S - \delta\right) \tag{6a}$$

$$I_R \propto \left(Q_1 E_1^2 + Q_2 E_2^2\right) + 2E_1 E_2 \cos\left(k_{SPP} S + \delta\right) \tag{6b}$$

where the $i = 1, 2$ subindex refers to the two columns that constitute the grating, which, as we recall, have their unit cells oriented at angles θ_1 and θ_2 to which the electric field components E_1 and E_2 couple. $Q_i \propto \cos\theta_i$ is the plasmonic conversion efficiency for each component, S is the lateral (along x-axis) column separation and k_{SPP} is the real part of the SPP propagation constant $\beta_{SPP} = \frac{\omega}{c}\sqrt{\frac{\varepsilon_d \varepsilon_m}{\varepsilon_d + \varepsilon_m}}$ (where ε_d is the dielectric constant in the dielectric medium and ε_m the one in the metallic medium). The phase difference between the components 1 and 2 of the electric field is given by δ.

Making the particular choice of lattice parameters $\theta_1 = 45°$ and $\theta_2 = 135°$ we have that $|\boldsymbol{E}_1|^2 + |\boldsymbol{E}_2|^2 = |\boldsymbol{E}|^2$ and $Q_1 = Q_2 = Q$. Furthermore, fixing $S = \frac{\pi}{2} k_{SPP}^{-1}$ yields

$$I_L \propto Q\left(E_1^2 + E_2^2\right) + 2E_1 E_2 \sin\left(\delta\right) \tag{7a}$$

$$I_R \propto Q\left(E_1^2 + E_2^2\right) - 2E_1 E_2 \sin\left(\delta\right) \tag{7b}$$

Thus, right and left plasmonic intensities depend on the phase difference between electric field components 1 and 2, and therefore on the polarization handedness of the incident wave.

3. Results and discussion

3.1. Chiral unit cell design

As described in Eq. (5), the absorption difference can be enhanced by increasing the chiral density of states while keeping the electric field enhancement low. This can be achieved by allowing larger enhancements of the magnetic field in the desired regions. A chiral HRI material S-like structure like the one shown in Fig. 2, can originate such enhancements due to the displacement currents originated in its curves upon interaction with CP light. Furthermore, its C2 rotation symmetry and elongated shape allows for dipole emission in the xy plane for a single component of an incident electric field, allowing the emission of directional plasmons in a double column pattern metasurface, as it will be shown later. The chosen HRI dielectric material is germanium. It allows to place the structure Mie resonances into the NIR region without enlarging the overall structure, which could hinder its operation within a double column pattern metasurface. The structure lays over glass ($n_g = 1.5$) and gold layers. The optical constants for Ge and Au were obtained from Palik [47] and Johnson & Christy [48] respectively. The introduction of the glass layer is motivated by the ease of fabrication of dielectric metasurfaces over glass or silica layers rather than metallic films [49]. The gold substrate considered here will act later as a platform for SPP launching.

In order to demonstrate the chiral enhancement given by this unit cell, the far-field CD signal, given by

$$CD(°) = \tan^{-1}\left(\frac{\sigma_{RCP} - \sigma_{LCP}}{\sigma_{RCP} + \sigma_{LCP}}\right) \tag{8}$$

was calculated alongside the extinction cross-sections (accounting for both scattering and absorption processes) for right-handed and left-handed CP cases σ_{RCP} and σ_{LCP}. The results were obtained by simulation with 3D-FDTD methods implemented with Lumerical FDTD. The results for the CD signal and the cross-sections can be observed in Fig. 3.

The identification of the cross-section resonances is complex given the convoluted geometry of the structure and illumination, but some of the resonances can be associated to the usual Mie theory modes, which for a Ge sphere of this size, correspond almost exclusively to dipolar resonances, due to the relevant absorption of the material below 1000 nm [50].

In general, resonances under CP illumination can be considered as a sum of the resonances upon linear polarization in the x and y axes. Due to the structure dimensions, the resonances for the x-polarization are found at shorter wavelengths than those in the y-polarization. Therefore, for CP illumination, an electric resonance can overlap with a magnetic one. These overlaps, especially evident for the x-polarized electric dipole (ED) and y-polarized secondary magnetic dipole (MD), are responsible for the differential extinction found in the [900, 1200] nm interval. The individual scattering and absorption cross-sections can be found in Fig. S1 of the Supplementary Document.

As for the CD signals obtained for different geometrical parameters, they are plotted in Fig. 4. The extinction cross-sections lead-

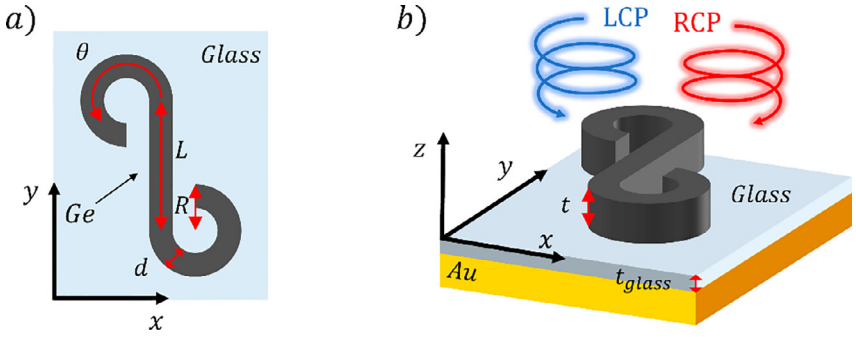

Fig. 2. a) Top view of the chiral S-like unit cell, where its geometrical parameters (L, d, R, θ) are shown. b) 3D view of the structure, where the gold and glass layers can be observed and the thicknesses (t, t_{glass}) are defined.

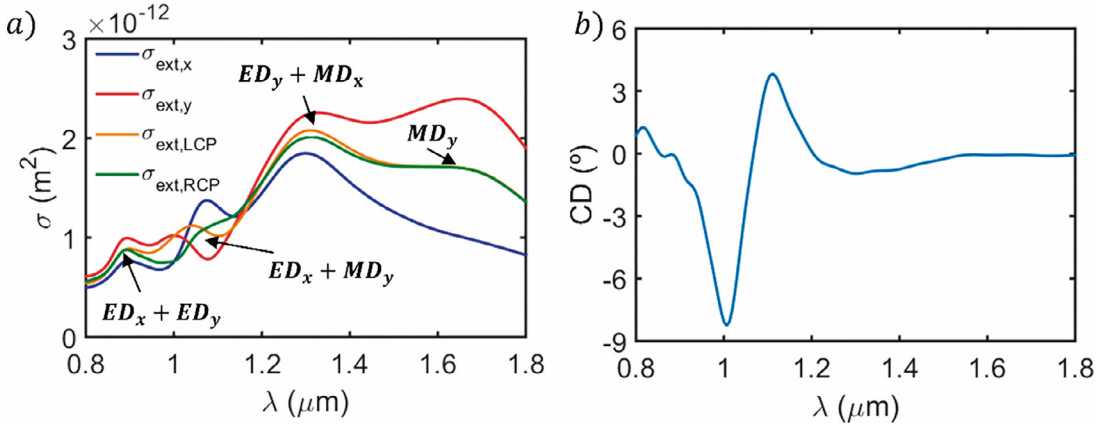

Fig. 3. a) Extinction cross sections of the proposed unit cell with geometrical parameters (L, d, R, t, d_{glass}) = (300, 60, 140, 300, 50) nm with $\theta = 240°$ upon interaction with x-polarized, y-polarized, RCP and LCP illuminations. Large extinction differences are found in the [900, 1200] nm interval, which leads to large non-zero values of the CD signal, shown in b). The extinction peaks in the CP resonances are identified according to Mie theory resonances.

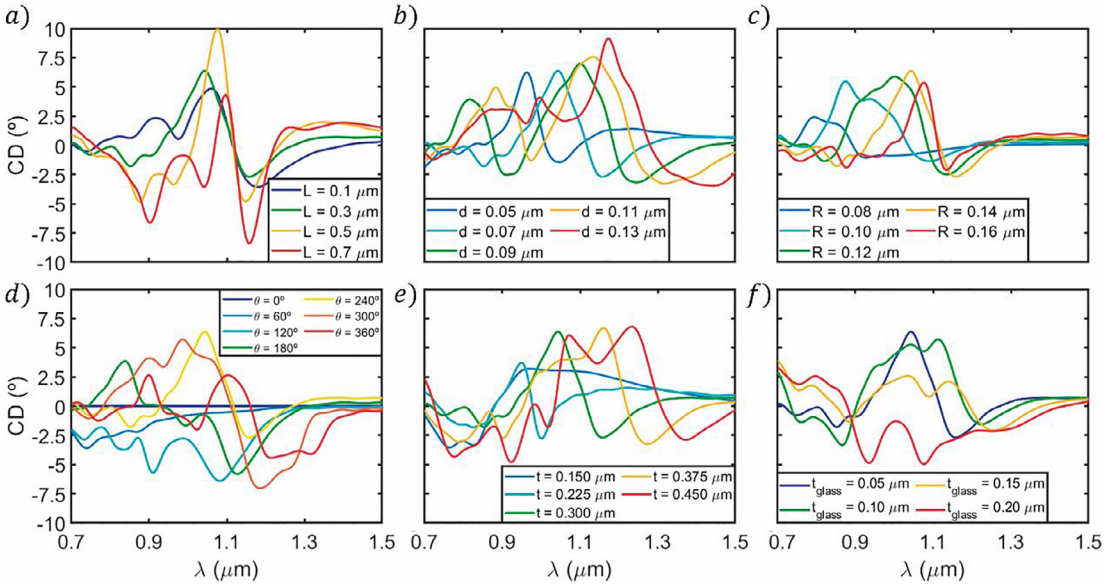

Fig. 4. CD signals upon variation of geometrical parameters in the unit cell structure. a) Central length L. b) Width d. c) Curve radius R. d) Angle θ. e) Height t. f) Glass layer thickness t_{glass}.

ing to these CD values can be found in Fig. S2 of the Supplementary Document. The behavior of CD when the geometrical parameters are varied is obviously complex due to the unusual particle shape and the not-linearly polarized incident field. Nevertheless, some common patterns can be recognized. For example, as the dimensions of the structure increase, the CD signal is generally redshifted. However, the wavelength shift of these resonances is different depending on the varied parameter. This means that some of these resonance peaks may combine or separate, causing strong variations on the overall absorption and therefore on the CD signal.

It can be seen that, as the central length L increases, the structure absorbs more, and the CD signal peaks increase, reaching maximum absolute values for $L = 500$ nm. A redshift can also be

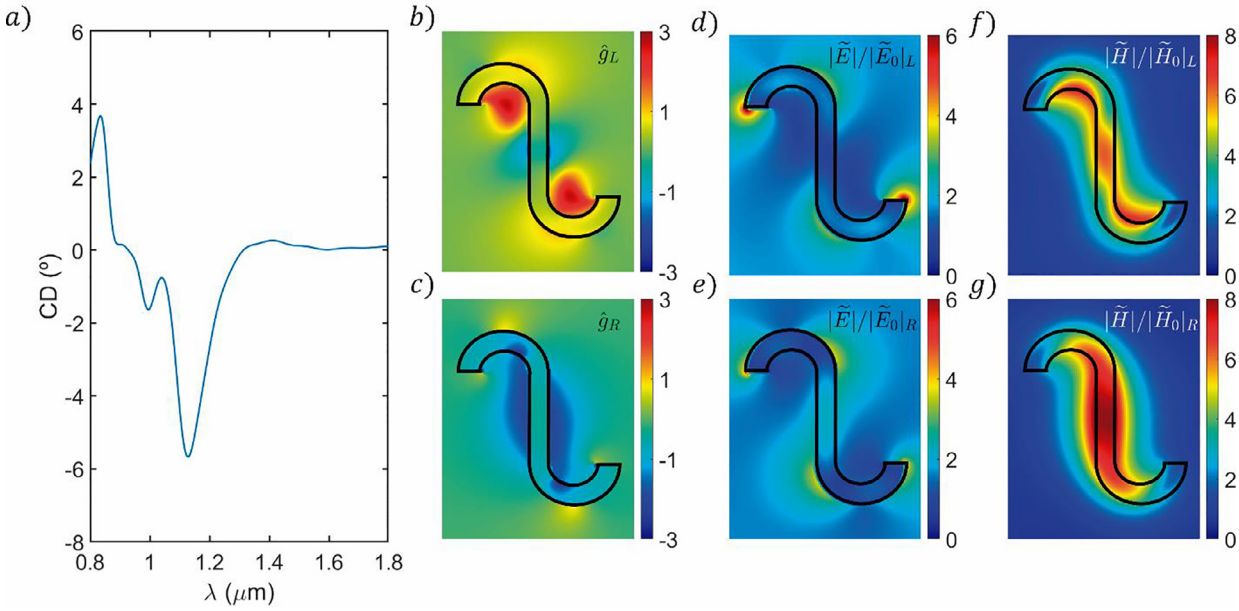

Fig. 5. a) CD signal of the optimal unit cell structure. b) and c) $\hat{g}$ values for LCP and RCP at the peak CD wavelength ($\lambda = 1130$ nm). d) and e) Near electric fields for LCP and RCP illuminations at the peak CD wavelength. f) and g) Near magnetic fields for LCP and RCP illuminations at the peak CD wavelength.

observed as the length increases, owing to the higher refractive index average, which displaces all resonances to higher wavelengths.

For the same reason, the increase in width of the structure d, leads to significant redshifts in the CD signal, but with almost no effect on its magnitude. Therefore, variation of this parameter allows to tune the structure spectral response. However, as big $\hat{g}$ factor enhancements are expected in the inner part of the curves, narrow structures are preferred in order to allocate more molecules.

Regarding the curves' radius R, a maximum absolute value is observed for $R = 140$ nm, with the respective redshift induced by the higher refractive index average in the case of larger curves. Again, larger radii are preferred as they offer larger areas to molecules.

Variation of the angle of curvature, θ, implies a severe change in how chiral the structure is, and therefore yields a complex behavior, including reversal of the CD signal for angles around 240°. It can be seen that for small angles, the structure resembles an achiral rod, and therefore offers very small CD enhancement. As the angle increases, the CD signal grows, reaching maximum absolute values at $\theta = 300°$.

Variation of the height of the structure t implies higher CD signals in principle, as there is more absorbing material Fig 3.e shows how thicker structures have generally larger and spectral redshifted values of the CD signal. However, the maximum value is similar owing to a CD peaks separation in the region $\lambda = 1100 - 1300$ nm. Finally, an increase in the thickness of the glass layer underneath the structure can also redshift the signal, up to a value $t_{glass} = 150$ nm. For larger values, the CD signal is reversed and a separation of peaks appears.

As explained before, directional plasmon emission requires the structure to emit as an electric dipole. Most of the configurations analyzed here do not have their CD maximum signal and ED resonances at the same wavelengths, therefore only a handful of configurations will be able to offer both chiral enhancement and directional plasmon emission. This can be clearly observed in the directional plasmon efficiency study shown in the Supplementary Document (Fig. S3).

For this reason, a system configuration with (L, d, R, t, d_{glass}) = (300, 70, 140, 300, 50) nm and $\theta = 180°$ was selected. The overall CD signal from this optimal unit cell can be observed in Fig. 5a. A peak value close to − 6° can be observed at a wavelength $\lambda = 1130$ nm. The cross-section results leading to this CD signal can be consulted in Fig. S4 of the Supplementary Document.

Fig. 5 d-g displays the near field results for this unit cell configuration at the maximum CD wavelength $\lambda = 1130$ nm. The LCP electric and magnetic near fields at this wavelength, shown in Fig. 5d and f, respectively, display large magnetic enhancement in the inner part of the curved regions with a small electric field enhancement, leading to a large enhancement of the g factor at those sites (Fig. 5b).

For RCP illumination, moderate field enhancements can be found at those sites (see Fig. 5e-g), with the magnetic field being concentrated on the center of the structure. This leads to lower values of the g factor (Fig. 5c), increasing the overall absorption difference. Furthermore, for both RCP and LCP, electric dipolar scattering can be found at the ends of the curves, with the RCP polarization also showing scattering in the vertical axis. Note that, while the electromagnetic response described here corresponds to one of the mirror images of the chiral structure, the other mirror image will display exactly the same response for opposite illumination handedness.

3.2. Directional plasmon source: study of the chiral unit cell in a double column metasurface

Once the chirality of the unit cell has been demonstrated, its capabilities as a directional plasmon source in the double-column metasurface must be analyzed. Following the pattern given in the literature [44] and shown in Figs. 6a and b with a period of $\Lambda = 1160$ nm, simulations of the metasurface upon interaction with RCP and LCP plane waves were done using Lumerical FDTD. The plasmon intensity was measured at both sides. The results, shown in Fig. 6c, prove that at a wavelength $\lambda = 1130$ nm for LCP illumination, plasmonic activity is almost only (86% of total plasmonic intensity obtained at both sides) found at the left of the structure, while the opposite result was found for the right-handed polarization. Near field maps (Fig. 6d and e) corresponding to the characteristic components of the electric field in SPPs E_z also support this result, with a clearly higher activity at the corresponding side of the metasurface.

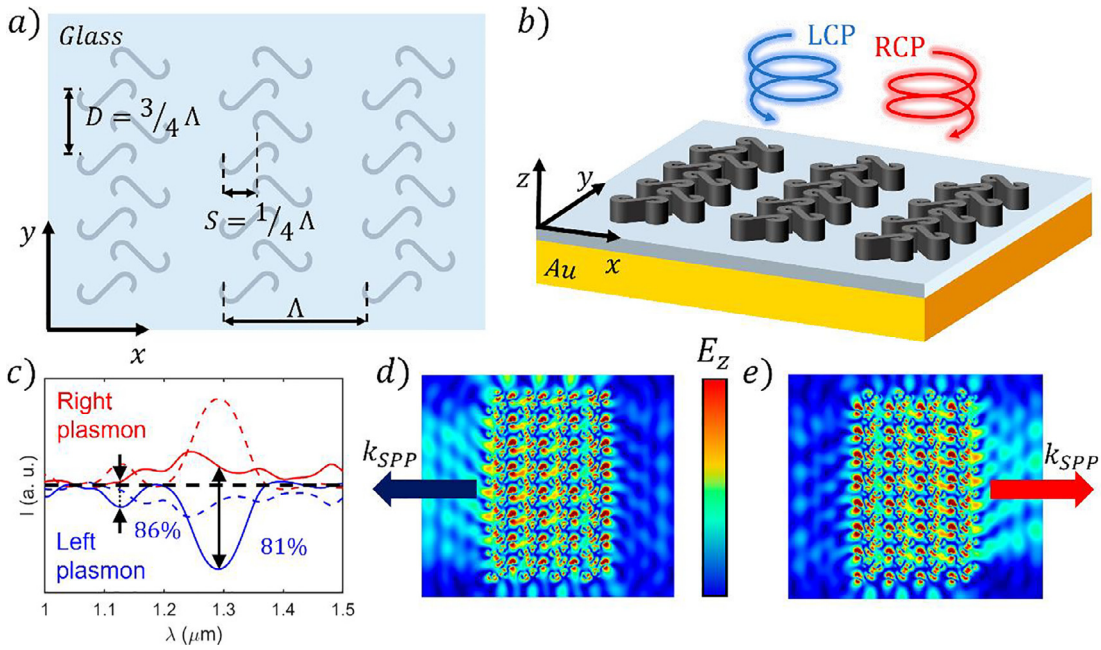

Fig. 6. a) Top view of the metasurface pattern, with its periodic characteristics defined. b) 3D view of the structure with the illumination scheme. c) Plasmonic activity measured for a metasurface formed by 4 double columns ($\Lambda = 1160$ nm) with 16 periods/column. The red and blue lines represent transmission of SPPs (positive values to the right, red, negative values to the left, blue) at plane monitors placed at 4.5 μm distance from the metasurface. The solid line represents LCP and the dashed line represents RCP illumination. An almost totally directional (86%) plasmon emission to the left is detected at a 1130 nm wavelength. d) and e) Near field map for the characteristic electric field SPP component (E_z) upon illumination with LCP and RCP light at a wavelength $\lambda = 1130$ nm, respectively.

A second more prominent peak can be observed at $\lambda = 1300$ nm. However, its plasmonic intensity at the opposite side is higher than in the first peak, making it less efficient in terms of directionality (81% vs 86% in the first peak). Furthermore, the mismatch between unit cell CD signal and the plasmonic peak wavelengths means that this particular peak would not be useful for chiral sensing applications.

It can also be seen that changes in the incident polarization handedness do not induce any changes in the differential plasmonic intensity, i.e., the plasmonic intensity obtained at the right for RCP is the same that the one at the left with LCP. This is due to the absence of analytes in the simulation. As the metasurface is racemic, the noise introduced by the chiral elements will be compensated by the equal number of right and left-handed unit cells. Thus, no absorption differences between polarizations will be found unless molecules are introduced into the system [22].

4. Conclusions

In this work, a proof of concept for a directional plasmonic chiral sensor has been given. Germanium S-shaped unit cells demonstrate an enhancement of the chiroptical interaction, yielding CD signals of around $-6°$ and a three-fold enhancement of the dissymmetry factor g at molecule-accessible sites. We show how tuning the Mie resonances of a HRI dielectric structure so that its CD signal matches the electric dipole resonances leads to directional emission of plasmons. This is demonstrated with the proposed unit cell structure at a double-column grating that mimics previous plasmonic works. These findings may establish the foundation of a brand-new path in chiral sensing and lead to other chiroptical applications.

Author contributions

G. S. and P. A. conceived the idea. G. S. and J. G-C. performed the FDTD numerical calculations. G. S., J. G-C., V. G. and P. A. carried out the theoretical interpretation. All authors participated in the analysis and discussion of the results. All the authors contributed to the writing of the manuscript. J. M. S. and P. A. supervised the work.

Declaration of Competing Interest

The authors declare no conflict of interest.

Acknowledgements

The authors gratefully acknowledge financial support from Spanish national project (No. PGC2018–096649-B-I). V. G. thanks the “ENSEMBLE3 - Centre of Excellence for nanophotonics, advanced materials and novel crystal growth-based technologies” project (GA No. MAB/2020/14) carried out within the International Research Agendas programme of the Foundation for Polish Science co-financed by the European Union under the European Regional Development Fund and the European Union’s Horizon 2020 research and innovation programme Teaming for Excellence (GA. No. 857543) for support of this work. G. S. thanks the Ministry of education for his collaboration grant. J. G-C and P. A thank the Ministry of science and Innovation of Spain for their grants, FPI and Ramon y Cajal Fellowship (No. RYC-2016–20831), respectively.

Supplementary materials

Supplementary material associated with this article can be found, in the online version, at doi:10.1016/j.jqsrt.2022.108166.

References

[1] Kelvin WTB. The molecular tactics of a crystal. Oxford: Clarendon; 1894.
[2] Kelvin WTB. Baltimore lectures on molecular dynamics and the wave theory of light. Cambridge: CJ Clay and Sons; 1904.
[3] Pasteur L. Memoire Sur La relation Qui Peut Exister Entre La Forme Cristalline Et La Composition Chimique, Et Sur La Cause De La Polarisation Rotatoire. Comptes Rendus Hebd Des Séances L’Academie Des Sci 1848;26:535.
[4] Mogilner A, Fogelson B. Cytoskeletal Chirality: swirling Cells Tell Left from Right. Curr Biol 2015;25:R501–3. doi:10.1016/J.CUB.2015.04.039.

[5] Hall JP, Keane PM, Beer H, Buvhner K, Winter G, Sorensen TL, et al. Delta chirality ruthenium "light-switch" complexes can bind in the minor groove of DNA with five different binding modes. Nucl Acids Res 2016;44:9472–82. doi:10.1093/NAR/GKW753.
[6] Dobson CM. Protein folding and misfolding. Nat 2003;426:884–90 2003 4266968. doi:10.1038/nature02261.
[7] Dally A. Thalidomide: was the tragedy preventable? Lancet 1998;351:1197–9. doi:10.1016/S0140-6736(97)09038-7.
[8] Baker J. The effects of drugs on the foetus. Pharmacol Rev 1960;12:37–90.
[9] Leslie F. Is thalidomide to blame? BMJ 1960;ii:1954.
[10] Nordén B. Circular dichroism and linear dichroism. Oxford: Oxford University Press; 1997.
[11] Yoo SJ, Park QH. Metamaterials and chiral sensing: a review of fundamentals and applications. Nanophotonics 2019;8:249–61. doi:10.1515/nanoph-2018-0167.
[12] Movsesyan A, Besteiro LV, Kong X-T, Wang Z, Govorov AO, Movsesyan A, et al. Engineering strongly chiral plasmonic lattices with achiral unit cells for sensing and photodetection. Adv Opt Mater 2021:2101943. doi:10.1002/ADOM.202101943.
[13] Nesterov ML, Yin X, Schäferling M, Giessen H, Weiss T. The role of plasmon-generated near fields for enhanced circular dichroism spectroscopy. ACS Photonics 2016;3:578–83. doi:10.1021/ACSPHOTONICS.5B00637.
[14] Kong X-T, Besteiro LV, Wang Z, Govorov AO. Plasmonic chirality and circular dichroism in bioassembled and nonbiological systems: theoretical background and recent progress. Adv Mater 2020;32:1801790. doi:10.1002/ADMA.201801790.
[15] Staude I, Sperrhake J, Decker M, Falkner M, Fasold S, Kaiser T, et al. Analyzing the polarization response of a chiral metasurface stack by semi-analytic modeling. Opt Express 2019;27(2):1236–48 Vol 271236–48. doi:10.1364/OE.27.001236.
[16] Tullius R, Platt GW, Khorashad LK, Gadegaard N, Lapthorn AJ, Rotello VM, et al. Superchiral Plasmonic phase sensitivity for fingerprinting of protein interface structure. ACS Nano 2017;11:12049–56. doi:10.1021/ACSNANO.7B04698.
[17] Wang X, Tang Z. Circular Dichroism Studies on Plasmonic Nanostructures. Small 2017;13:1601115. doi:10.1002/SMLL.201601115.
[18] González-Rubio G, Mosquera J, Kumar V, Pedrazo-Tardajos A, Llombart P, Solís DM, et al. Micelle-directed chiral seeded growth on anisotropic gold nanocrystals. Science (80-) 2020;368:1472–7. doi:10.1126/science.aba0980.
[19] Pedrueza-Villalmanzo E, Pineider F, Dmitriev A. Perspective: plasmon antennas for nanoscale chiral chemistry. Nanophotonics 2020;9:481–9. doi:10.1515/nanoph-2019-0430.
[20] Luo Y, Chi C, Jiang M, Li R, Zu S, Li Y, et al. Plasmonic chiral nanostructures: chiroptical effects and applications. Adv Opt Mater 2017;5:1–18. doi:10.1002/adom.201700040.
[21] Murugkar S, De Leon I, Horton M, Qassim H, Leach J, Boyd RW. Planar chiral metamaterials for biosensing applications. Plasmon Biol Med X 2013;8597:85970Y. doi:10.1117/12.2004748.
[22] García-Guirado J, Svedendahl M, Puigdollers J, Quidant R. Enantiomer-Selective Molecular Sensing Using Racemic Nanoplasmonic Arrays. Nano Lett 2018;18:6279–85. doi:10.1021/acs.nanolett.8b02433.
[23] Barreda AI, Saiz JM, González F, Moreno F, Albella P. Recent advances in high refractive index dielectric nanoantennas: basics and applications. AIP Adv 2019;9:040701. doi:10.1063/1.5087402.
[24] Evlyukhin AB, Reinhardt C, Seidel A, Luk'Yanchuk BS, Chichkov BN. Optical response features of Si-nanoparticle arrays. Phys Rev B - Condens Matter Mater Phys 2010;82:045404. doi:10.1103/PHYSREVB.82.045404/FIGURES/15/MEDIUM.
[25] García-Etxarri A, Gómez-Medina R, Froufe-Pérez LS, López C, Chantada L, Scheffold F, et al. Strong magnetic response of submicron Silicon particles in the infrared. Opt Express 2011;19(6):4815–26 Vol 194815–26. doi:10.1364/OE.19.004815.
[26] Evlyukhin AB, Novikov SM, Zywietz U, Eriksen RL, Reinhardt C, Bozhevolnyi SI, et al. Demonstration of magnetic dipole resonances of dielectric nanospheres in the visible region. Nano Lett 2012;12:3749–55. doi:10.1021/NL301594S.
[27] Kuznetsov AI, Miroshnichenko AE, Fu YH, Zhang J, Lukyanchukl B. Magnetic light. Sci Reports 2012;2:1–6 2012 21. doi:10.1038/srep00492.
[28] Albella P, Poyli MA, Schmidt MK, Maier SA, Moreno F, Sáenz JJ, et al. Low-loss electric and magnetic field-enhanced spectroscopy with subwavelength silicon dimers. J Phys Chem C 2013;117:13573–84. doi:10.1021/JP4027018.
[29] Miroshnichenko AE, Evlyukhin AB, Yu YF, Bakker RM, Chipouline A, Kuznetsov AI, et al. Nonradiating anapole modes in dielectric nanoparticles. Nat Commun 2015;6:1–8 2015 61. doi:10.1038/ncomms9069.
[30] Kuznetsov AI, Miroshnichenko AE, Brongersma ML, Kivshar YS, Luk'yanchuk B. Optically resonant dielectric nanostructures. Science 2016;354(80–). doi:10.1126/SCIENCE.AAG2472.
[31] Shibanuma T, Grinblat G, Albella P, Maier SA. Efficient third harmonic generation from metal–dielectric hybrid Nanoantennas. Nano Lett 2017;17:2647–51. doi:10.1021/ACS.NANOLETT.7B00462.
[32] Krasnok AE, Simovski CR, Belov PA, Kivshar YS. Superdirective dielectric nanoantennas. Nanoscale 2014;6:7354–61. doi:10.1039/C4NR01231C.
[33] Ma Z, Li Y, Li Y, Gong Y, Maier SA, Hong M. All-dielectric planar chiral metasurface with gradient geometric phase. Opt Express 2018;26:6067. doi:10.1364/oe.26.006067.
[34] Gómez FR, Mejía-Salazar JR, Albella P. All-dielectric chiral metasurfaces based on crossed-bowtie nanoantennas. ACS Omega 2019;4:21041–7. doi:10.1021/acsomega.9b02381.
[35] Hu J, Zhao X, Lin Y, Zhu A, Zhu X, Guo P, et al. All-dielectric metasurface circular dichroism waveplate. Sci Rep 2017;7:1–9. doi:10.1038/srep41893.
[36] Droulias S, Bougas L. Absolute chiral sensing in dielectric metasurfaces using signal reversals. Nano Lett 2020;20:5960–6. doi:10.1021/acs.nanolett.0c01938.
[37] Reyes Gómez F, Oliveira ON, Albella P, Mejía-Salazar JR. Enhanced chiroptical activity with slotted high refractive index dielectric nanodisks. Phys Rev B 2020;101:1–6. doi:10.1103/PhysRevB.101.155403.
[38] Solomon ML, Saleh AAE, Poulikakos LV, Abendroth JM, Tadesse LF, Dionne JA. Nanophotonic platforms for chiral sensing and separation. Acc Chem Res 2020;53:588–98. doi:10.1021/acs.accounts.9b00460.
[39] Nguyen HH, Park J, Kang S, Kim M. Surface plasmon resonance: a versatile technique for biosensor applications. Sensors (Basel) 2015;15:10481–510. doi:10.3390/S150510481.
[40] Schasfoort RBM. Handbook of surface plasmon resonance. R Soc Chem; 2017. doi:10.1039/9781788010283.
[41] Nylander C, Liedberg B, Lind T. Gas detection by means of surface plasmon resonance. Sensors Actuators 1982;3:79–88. doi:10.1016/0250-6874(82)80008-5.
[42] González-Colsa J, Serrera G, Saiz JM, González F, Moreno F, Albella P. On the performance of a tunable grating-based high sensitivity unidirectional plasmonic sensor. Opt Express 2021;29(9):13733–45 Vol 2913733–45. doi:10.1364/OE.422026.
[43] Droulias S, Bougas L. Surface Plasmon Platform for Angle-Resolved Chiral Sensing. ACS Photonics 2019;6:1485–92. doi:10.1021/acsphotonics.9b00137.
[44] Lin J, Mueller JPB, Wang Q, Yuan G, Antoniou N, Yuan XC, et al. Polarization-controlled tunable directional coupling of surface plasmon polaritons. Science (80-) 2013;340:331–4. doi:10.1126/science.1233746.
[45] Tang Y, Cohen AE. Optical chirality and its interaction with matter. Phys Rev Lett 2010;104:1–4. doi:10.1103/PhysRevLett.104.163901.
[46] Tang Y, Cohen AE. Enhanced enantioselectivity in excitation of chiral molecules by superchiral light. Science (80-) 2011;332:333–6. doi:10.1126/SCIENCE.1202817.
[47] Palik ED. Handbook of optical constants of solids. Amsterdam: Elsevier; 1985.
[48] Johnson PB, Christy RW. Optical constants of the noble metals. Phys Rev B 1972;6:4370. doi:10.1103/PhysRevB.6.4370.
[49] Aouani H, Wenger J, Gérard D, Rigneault H, Devaux E, Ebbesen TW, et al. Crucial role of the adhesion layer on the plasmonic fluorescence enhancement. ACS Nano 2009;3:2043–8. doi:10.1021/NN900460T.
[50] García-Cámara B, Gómez-Medina R, Sáenz JJ, Sepúlveda B. Sensing with magnetic dipolar resonances in semiconductor nanospheres. Opt Express 2013;21:23007. doi:10.1364/oe.21.023007.